Polymer Journal (2013) 45, 193–201

www.nature.com/pj

ORIGINAL ARTICLE

Influence of the primary structure of the main chain on backbone stiffness of cylindrical rod brushes

Yuta Saito[1], Le Thi Ngoc Lien[1], Yuji Jinbo[2], Jiro Kumaki[1], Atsushi Narumi[1] and Seigou Kawaguchi[1]

The dimensional properties of rod brushes consisting of a flexible polymethacrylate main chain and poly(*n*-hexyl isocyanate; PHIC) rod side chains have been studied using static light and small-angle X-ray scattering (SAXS) techniques in tetrahydrofuran (THF) at 25 °C. The results are compared with those consisting of a flexible polystyrene main chain and PHIC side chains (VB-HIC-N_s-H, where N_s is the weight-averaged degree of polymerization of HIC). The rod brushes were prepared through the radical homopolymerizations of α-methacryloyloxyethoxy-ω-acetyl-PHIC macromonomer (MA-HIC-*61*-Ac) in *n*-hexane at 60 °C. The molecular weight dependence of the z-averaged mean-square radius of gyration ($\langle R_g^2 \rangle_z$) of the brush is quantitatively described in terms of the wormlike cylinder model taking into account the end effects. The main chain stiffness parameter (λ_M^{-1}) is determined to be 197 nm for poly(MA-HIC-*61*-Ac), which is approximately three times greater than that for poly(VB-HIC-*62*-H), which has a polystyrene main chain and the same rod length. The considerably larger stiffness in the polymethacrylate than in the polystyrene is most likely responsible for the larger effective excluded volume effects produced by the freely rotating spacer between the main chain and side rod. A single rod brush of poly(MA-HIC-*61*-Ac) on a mica surface is clearly observed using atomic force microscopy to reasonably demonstrate the cylindrical rod brushes.
Polymer Journal (2013) **45,** 193–201; doi:10.1038/pj.2012.117; published online 20 June 2012

Keywords: chain stiffness; cylindrical rod brushes; polymacromonomers; poly(*n*-hexyl isocyanate); radius of gyration; SAXS; SEC-MALS

INTRODUCTION

Over the past two decades, poly(macromonomer)s, molecular bottlebrushes and cylindrical polymer brushes, which have one of the best defined comb-branched architectures, have gained increasing attention.[1–5] This interest arises because of potential applications that range from nanotechnology (for example, photonic crystals,[6–8] nanotubes[9] and nanowires[10] precursors) to biomedical applications (for example, drug delivery carriers).[11,12] A variety of homo- and copolymer bottlebrushes with single-component or core-shell side chains have currently been synthesized using grafting from,[13] grafting onto,[14] and grafting through techniques with varying degrees of grafting efficiency.[15] Recently, the great progress in controlled living radical polymerization and click chemistry allows for the preparation of a variety of polymers with complex architectures.[16] Grafting through, which is a 'macromonomer' method, has an advantage because the grafted chains are predetermined.[4] The macromonomer homopolymerizes under an appropriate condition to produce a well-defined star- or comb-shaped polymer, depending on the degree of polymerization of the main chain.[4]

Considerably fewer fundamental studies on the physicochemical properties of the brushes, however, have been reported compared with the many reports on the synthesis and applications of the brushes. One interesting and very valuable finding about the conformational properties of the brushes is that the main chain remarkably stiffens in a dilute solution and the solid state, despite being originally composed of flexible chains.[17–28] Schmidt *et al.*,[17–19] and Terao and Nakamura *et al.*[20–24] have reported that the main chain stiffness parameter (λ_M^{-1}) of the 'flexible brushes' increases with increasing length of the side chain and solvent power. These stiffening effects may arise from the repulsive interactions (excluded volume effects) among the densely packed side chains.[23,24]

In our previous papers,[29,30] we have reported the molecular characterizations of another class of brushes, the so-called 'rod brushes', which consist of a flexible polystyrene backbone and poly(*n*-hexyl isocyanate; PHIC) semi-flexible or rod chains. Interestingly, there is a considerably higher main chain stiffness in the rod brushes than in the flexible brushes with the same contour length of the side chain. This observation is believed to arise from the larger excluded volume effects produced among the side rods. This result also implies that the chemical nature, that is, the individuality of the side chain, strongly influences the main chain flexibilities of the brushes throughout the extent of the excluded volume effects among the side chains. Because

[1]Department of Polymer Science and Engineering, Graduate School of Science and Engineering, Yamagata University, Jonan, Yonezawa, Japan and [2]Department of Biochemical Engineering, Graduate School of Science and Engineering, Yamagata University, Yonezawa, Japan
Correspondence: Professor S Kawaguchi, Department of Polymer Science and Engineering, Graduate School of Science and Engineering, Yamagata University, 4-3-16, Jonan, Yonezawa, Yamagata 992-8510, Japan.
E-mail: skawagu@yz.yamagata-u.ac.jp
Received 10 April 2012; revised 23 April 2012; accepted 24 April 2012; published online 20 June 2012

of these observations, our interest concerns how the difference in the primary structure of the main chain is influenced by the side chain.

In this paper, we report the dilute solution properties of PHIC rod brushes consisting of a polymethacrylate chain in THF at 25 °C determined using small-angle X-ray scattering (SAXS) and light scattering, as shown in Scheme 1. The experimental results are compared with rod brushes that have a polystyrene main chain and the same PHIC rods to experimentally clarify the influence of the primary structure of main chain on the conformation of the rod brushes.

EXPERIMENTAL PROCEDURE

Materials

Benzene (Kanto Chemical Co., Tokyo, Japan) was purified by washing with concentrated H_2SO_4, water and sodium hydroxide solution, and then dried with calcium chloride, followed by distilling from a sodium/benzophenone ketyl solution. Tetrahydrofuran (THF; Kanto Chemical Co.) was also purified by distillation from a sodium/benzophenone ketyl solution. Dichloromethane (Kanto Chemical Co.) and *n*-hexane (Kanto Chemical Co.) were distilled over CaH_2 before use. Methanol (Wako Pure Chemical Industries, Osaka, Japan) was used as received. *n*-Hexyl isocyanate (HIC; Tokyo Chemical Industry Co., Ltd, Tokyo, Japan), methyl methacrylate (MMA; Wako Pure Chemical Industries) and acetic anhydride (Kanto Chemical Co.) were distilled from CaH_2 under reduced pressure just before use. 2-Hydroxyethyl methacrylate (HEMA; Kanto Chemical Co.) was distilled under reduced pressure before use. Trichlorocyclopentadienyl titanium (Kanto Chemical Co.) and boron trifluoride-diethyl etherate (Kanto Chemical Co.) were used as received. The radical initiator, dimethyl-2, 2′-azobis(2-methyl proionate); V601 (Wako Pure Chemical Industries), was used as received, and 2, 2′-azobis(isobutyronitrile); AIBN (Wako Pure Chemical Industries) was purified by recrystallization three times from methanol. Poly(MMA) standards ($M_p = 1.25 \times 10^6\,g\,mol^{-1}$, $M_w/M_n = 1.07$, $M_p = 6.59 \times 10^5\,g\,mol^{-1}$, $M_w/M_n = 1.02$, $M_p = 3.00 \times 10^5\,g\,mol^{-1}$, $M_w/M_n = 1.02$ and $M_p = 1.39 \times 10^5\ g\,mol^{-1}$, $M_w/M_n = 1.05$) were purchased from Polymer Laboratories Ltd, Shropshire, UK and used as received. Spectroscopic grade THF (Kanto Chemical Co.) and acetone (Kanto Chemical Co.) were used for the refractive index increment (d*n*/d*c*) and SAXS measurements. Unless otherwise specified, all other reagents were purchased from commercially available sources and used as received.

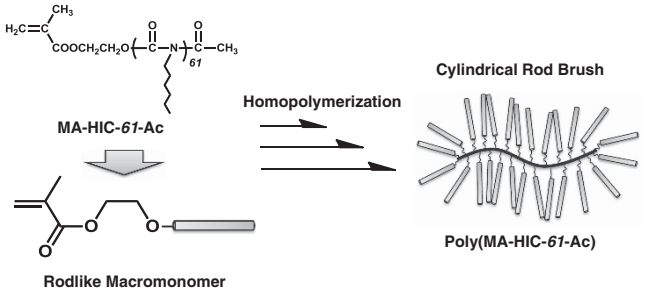

Scheme 1 Chemical and schematic structure of the cylindrical rod brushes consisting of a polymethacrylate main chain and PHIC side rods.

Preparation of PHIC macromonomer (MA-HIC-*61*-Ac)

α-Methacrylate-ω-acetyl ended PHIC macromonomer (MA-HIC-*61*-Ac, where *61* is the weight-averaged degree of polymerization of HIC) was prepared using the initiator method of living coordination polymerization of HIC using 2-methacryloyloxyethoxydichloro(cyclopentadienyl) titanium (IV); HEMACpTiCl$_2$ as an initiator, as shown in Scheme 2. The details of the preparation and characterization of the macromonomer have been described in previous papers.[31–33] Briefly, the initiator, HEMACpTiCl$_2$, was synthesized as follows. In a dry box, a solution of HEMA (4.56 mmol) in 5 ml of dry THF was slowly added to a solution of trichlorocyclopentadienyl titanium (4.56 mmol) in 5 ml of dry THF in a 50 ml three-necked flask with a magnetic stir bar and a tube containing dry triethylamine to trap the produced HCl. The reaction was conducted at room temperature for 24 h, and then the reaction mixture was evaporated. Finally, the product was dissolved in 15 ml of dry benzene and then freeze dried to produce a yellow solid (yield = 89–95%). The polymerization of HIC was also performed in a dry box. HEMACpTiCl$_2$ and dichloromethane were added to a 20 ml flask containing a magnetic stirrer bar. After the initiator was completely dissolved, a desired amount of HIC was added and the flask was sealed off and then removed from the dry box. The polymerization proceeded for 18 h at room temperature to yield a PHIC living chain as a solid material. The ω-end-functionalization of the PHIC living chain by acetic anhydride was performed using a heterogeneous reaction to avoid a back-biting reaction during the termination. Accordingly, the solution containing 500 times the equivalent amount of acetic anhydride and 20

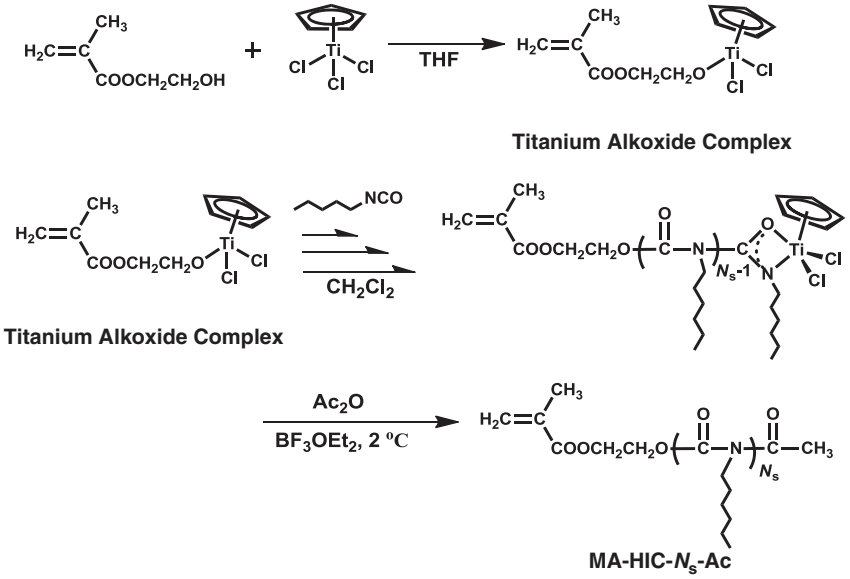

Scheme 2 Synthetic schemes of the MA-HIC-N_s-Ac macromonomers.

times the equivalent amount of boron trifluoride-diethyl etherate to the initiator was added to the solid reaction mixtures, which were prepared as described above, in a dry box. The solid was pulverized in the reaction mixture to disperse it. The dispersion was vigorously stirred at room temperature for 24 h at 2 °C. After the reaction, the polymer dispersion was slowly poured into a large excess of methanol at −70 °C. The precipitate was filtered and redissolved into THF containing 5% methanol and then reprecipitated into methanol. This procedure was performed three times, and the polymer was finally freeze dried from the benzene solution.

Homopolymerization of MA-HIC-*61*-Ac and MMA

The polymacromonomer sample, poly(MA-HIC-*61*-Ac), was prepared in a sealable ampoule from the radical homopolymerization of MA-HIC-*61*-Ac using dimethyl-2, 2′-azobis(2-methyl propionate); V-601 as an initiator in *n*-hexane at 60 °C for 24 h. After polymerization, the reaction mixture was dissolved into THF and precipitated into methanol, followed by washing five times with *n*-hexane to completely remove the unreacted (unpolymerized) macromonomer.[29] Finally, the polymer was dissolved in dry benzene and then freeze dried. The content of a typical reaction was [macromonomer] $= 50.6\,\mathrm{mmol\,l^{-1}}$ and $[\text{V-601}] = 8.0\,\mathrm{mmol\,l^{-1}}$, and the polymerization yielded 61% in the conversion (differential refractive index signal ratio in size exclusion chromatography (SEC)) with a $M_w = 8.2 \times 10^6$ (SEC-multiangle laser light scattering (MALS)). The linear PMMA with a molecular weight greater than 10^6 was prepared in a sealable ampoule through the radical polymerization of MMA with 2, 2′-azobis(isobutyronitrile); AIBN as an initiator in benzene at 60 °C for 3–24 h. After polymerization, the reaction mixture was dissolved into THF and precipitated into methanol. Finally, the polymer was dissolved in dry benzene and then freeze dried. The contents of a typical reaction were $[\text{MMA}] = 4.7\,\mathrm{mol\,l^{-1}}$ and $[\text{AIBN}] = 8.7\,\mathrm{mmol\,l^{-1}}$, and the polymerization yield was 85% during the conversion with a $M_w = 3.6 \times 10^5$ (determined by SEC-MALS). The triad tacticities of the prepared PMMA were measured using ^{1}H nuclear magnetic resonance spectroscopy and were found to be $mm = 0.0360$, $mr = 0.346$ and $rr = 0.618$, which are somewhat different from those of the PMMA standard sample ($mm = 0.0170$, $mr = 0.158$ and $rr = 0.825$).

MEASUREMENTS

The weight-averaged molecular weight (M_w) and z-averaged mean-square radius of gyration ($\langle R_g^2 \rangle_z$) of poly(MA-HIC-*61*-Ac) and PMMA were determined using SEC-MALS (eluent: THF; flow rate: $1.0\,\mathrm{ml\,min^{-1}}$; 40 °C; columns: Shodex KF802 + KF806L + KF806L + KF806L, degasser; Tosoh SD-8022, pump; Tosoh SD-8020, RI; Tosoh RI-8020 and UV; Tosoh UV-8020, Tosoh Co., Tokyo, Japan), equipped with a MALS detector (DAWN-DSP, Wyatt Technology, Santa Barbara, CA, USA, wavelength $\lambda = 632.8$ nm) at 25 °C. The Rayleigh ratio, $R(90)$, at a scattered angle of 90° was based on that of pure toluene at a wavelength of 632.8 nm at 25 °C. The corrections for the sensitivity and scattering volume of the 17 detectors at angles of other than 90° and the dead volume for each detector were performed using the scattering intensities of a 0.30 wt% THF solution of a polystyrene standard with a $M_w = 1.67 \times 10^4\,\mathrm{g\,mol^{-1}}$ and $M_w/M_n = 1.05$.[30] The polymer sample solutions with a mass concentration (C_p) of approximately $5 \times 10^{-4}\,\mathrm{g\,ml^{-1}}$ were injected using a sample loop of 100 µl to the SEC columns and then diluted to a concentration that was 10–10^3 times lower than the original C_p in the columns during the separation. Therefore, the concentration effects on the values of M_w and $\langle R_g^2 \rangle_z$ can be ignored.[30]

The specific refractive index increment (d*n*/d*c*) of poly(MA-HIC-*61*-Ac) and PMMA in spectroscopic grade THF at 25 °C was measured using a differential refractometer (DRM-1021, Otsuka Electronics, Co., Ltd, Osaka, Japan, wavelength $\lambda = 632.8$ nm). All sample solutions were prepared using the gravimetric method. The weight fraction, W_p, is then converted to C_p ($\mathrm{g\,ml^{-1}}$) using the following equation:

$$C_p\,(\mathrm{g\,ml^{-1}}) = \frac{W_p}{\rho_0^{-1}(1 - W_p) + vW_p} \quad (1)$$

where ρ_0 is the density of the pure solvent ($0.8830\,\mathrm{g\,ml^{-1}}$ for THF at 25 °C) and v is the partial specific volume of PHIC, which was determined using a DMA 4500 M densimeter (Anton Paar GmbH, Graz, Austria), and was found to be $0.967\,\mathrm{ml\,g^{-1}}$ at 25 °C.

SAXS measurements were performed at 25 °C using a NANO-Viewer (Rigaku Co., Tokyo, Japan) as an X-ray source. The wavelength of the X-rays was 1.5418 Å. The scattering intensities were recorded using a High-Speed 2D X-ray Detector DECTRIS 100 k PILATUS (DECTRIS Ltd, Baden, Switzerland). The scattered vector was calibrated using a lead stearate.

The atomic force microscopy (AFM) measurements were performed using a Nanoscope III and IV with a multimode AFM unit (Veeco Instruments Inc., Santa Barbara, CA, USA) in air at room temperature with standard silicon cantilevers (NCH, NanoWorld, Neuchâtel, Switzerland) in the tapping mode. The samples for the AFM measurements were prepared by spin casting a drop of THF solution ($W_p = 3.0 \times 10^{-6}$ w/w) onto freshly cleaved mica at 2000 r.p.m. The measurement conditions were 1–1.3 V target amplitude, 500 nm scan size, 1.8–1.97 Hz scan rate and 0.745–1.0 V amplitude set point.

The ^{1}H nuclear magnetic resonance spectrum was recorded using a JNM-ECX400 (JEOL Ltd, Tokyo, Japan) instrument.

RESULTS AND DISCUSSION

The characteristics of the synthesized α-methacryloyloxyethoxy-ω-acetyl PHIC macromonomer, MA-HIC-*61*-Ac are listed in Table 1, along with those of the α-4-vinylbenzyloxy-ω-hydrogen terminated PHIC macromonomer (VB-HIC-*62*-H), for comparison. The molecular weight and molecular weight distribution of MA-HIC-*61*-Ac were determined from the SEC measurement that was calibrated with a series of PHICs as a standard.[29] The synthetic yield is 82.3%, and the ω-end functionality that was determined from the ratio of the ^{1}H nuclear magnetic resonance peak intensities of an ω-acetyl group to the ethoxy group of an α-HEMA terminal group is quantitative (100%).

In the following, we first report the dimensional properties of the linear PMMA in THF at 25 °C as a linear counterpart of poly (MA-HIC-*61*-Ac). Then, many details of the conformational properties of the poly(MA-HIC-*61*-Ac) chain in THF are reported and compared with those of the rod brush that has a polystyrene backbone and the same side rod length, poly(VB-HIC-*62*-H).

M_w dependence of radius of gyration of linear PMMA

Figure 1 shows the square root plots of $P(q)^{-1/2}$ versus q^2 obtained from the SEC-MALS measurements in THF at 25 °C for the PMMA

Table 1 Characteristics of MA-HIC-*61*-Ac macromonomer prepared in this study

Sample	$M_w \times 10^3$ [a] ($\mathrm{g\,mol^{-1}}$)	N_s [b]	M_w/M_n [a]
MA-HIC-*61*-Ac	7.94	61	1.2_5
VB-HIC-*62*-H[30]	8.04	62	1.1_6

Abbreviations: PHIC, poly(*n*-hexyl isocyanate); SEC, size exclusion chromatography.
[a]Determined by SEC calibrated with a series of PHICs as a standard.
[b]Weight-averaged degree of polymerization of HIC.

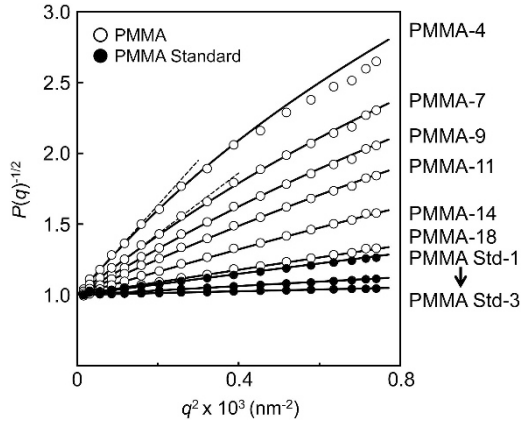

Figure 1 Angular dependence of $P(q)^{-1/2}$ for the indicated fractions of PMMA prepared by radical polymerization (○) and PMMA standards (●) in THF at 25 °C. The broken lines show the initial slope, and the solid curves are calculated from the Debye function.

with the broad molecular weight distribution (○) and three PMMA standards with narrow molecular weight distribution (●), where $P(q)$ denotes the single particle scattering function. From the initial slope (represented by broken lines) in these plots, the z-averaged mean-square radius of gyration $\langle R_g^2 \rangle_z^{1/2}$ is determined via the following equation:

$$P(q)^{-1/2} = 1 + \frac{1}{6}\langle R_g^2 \rangle_z q^2 + \cdots, \text{ and } q = \frac{4\pi n_0 \sin(\theta/2)}{\lambda} \qquad (2)$$

where n_0 is the refractive index of THF, θ is the scattering angle and λ is the wavelength of the incident light. The solid lines in this figure are the theoretical $P(q)$ from the Debye function for the Gaussian chain, which is defined by the equation:

$$P(q) = \left(\frac{2}{x^2}\right)[\exp(-x) - 1 + x] \text{ and } x = \langle R_g^2 \rangle q^2 \qquad (3)$$

The experimental $P(q)$ of each fraction that was separated by SEC and the PMMA standard are at most described in terms of the Debye function at least within the q range examined, supporting the precise determination of the M_w and $\langle R_g^2 \rangle_z$ values for each fraction fractionated by the SEC mode. Note that the particle scattering function of PMMA is better fitted with the helical wormlike chain than with the Debye function.[34] The molecular characteristics of PMMA in THF at 25 °C are summarized in Table 2.

Figure 2 shows the double logarithmic plot of $\langle R_g^2 \rangle_z^{1/2}$ versus M_w for PMMA in THF at 25 °C. Note that in this figure, the experimental data (○) from the PMMA prepared using radical polymerizations are superimposed on those of the PMMA standards (●) within experimental error. Accordingly, the SEC-MALS method is a reliable and powerful technique for the direct determination of M_w and $\langle R_g^2 \rangle_z$ of linear polymers that have a broad molecular weight distribution, as in the case of linear polystyrene.[35] Another interesting point to highlight is the tacticity difference. The PMMA samples studied here are essentially atactic; however, there is a slight difference between the PMMA standards and PMMA prepared using radical polymerization, as described in the experimental section. The former has higher *racemo* diad (that is, syndiotactic rich; $r = 0.90$) than the latter ($r = 0.79$). As observed in this figure, the influence of this slight difference in the tacticity on the conformation of PMMA may be essentially ignored in the region where the M_w is $>10^5$. The experimental M_w dependence of $\langle R_g^2 \rangle_z^{1/2}$ may be given by the

Table 2 Characterization results of PMMA's prepared by radical polymerization and PMMA standards

Slice number of PMMA	$M_w \times 10^{-6}$[a] (g mol^{-1})	$N_M \times 10^{-3}$[b]	$\langle R_g^2 \rangle_z^{1/2}$[a] (nm)
1	9.48	94.8	158
2	8.44	84.4	145
3	8.09	80.9	144
4	7.59	75.9	138
5	6.93	69.3	130
6	6.34	63.4	123
7	5.67	56.7	114
8	5.10	51.0	107
9	4.50	45.0	99.6
10	3.95	39.5	91.7
11	3.58	35.8	87.1
12	3.19	31.9	81.9
13	2.82	28.2	75.9
14	2.48	24.8	70.1
15	2.16	21.6	63.7
16	1.90	19.0	59.7
17	1.68	16.8	55.6
18	1.47	14.7	51.7
19	1.25	12.5	46.5
20	0.705	7.05	32.7
21	0.619	6.19	30.3
22	0.541	5.41	27.9
23	0.472	4.72	26.0
Standard-1	1.29[c]	12.9	47.4[c]
Standard-2	0.632[c]	6.32	30.7[c]
Standard-3	0.296[c]	2.96	19.6[c]
Standard-4	0.142[c]	1.42	12.6[c]

Abbreviations: MALS, multiangle laser light scattering; PMMA, poly(methyl methacrylate); SEC, size exclusion chromatography; THF, tetrahydrofuran.
[a]Determined by SEC-MALS in THF at 25 °C.
[b]Weight-averaged degree of polymerization.
[c]Value of the peak top in SEC-MALS chromatogram.

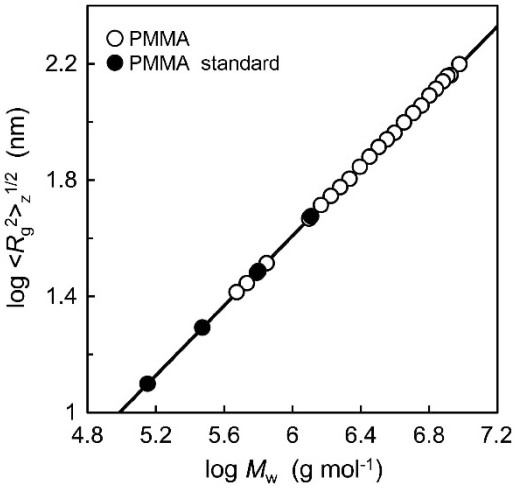

Figure 2 Double-logarithmic plot of $\langle R_g^2 \rangle_z^{1/2}$ versus M_w for PMMA (○) in THF at 25 °C, together with the data of the PMMA std. (●) in THF at 25 °C. The solid line is calculated from Equation (4).

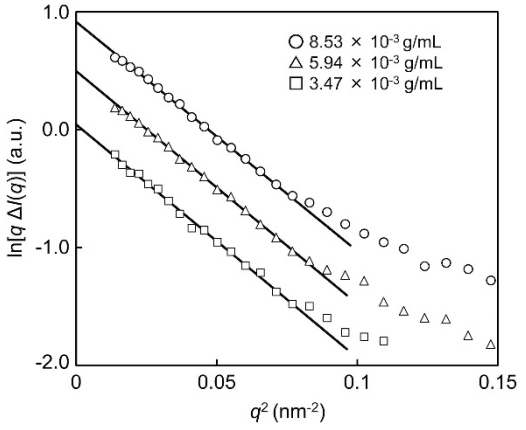

Figure 3 Cross-sectional Guinier plots of $\ln(q\Delta I(q))$ as a function q^2 for poly(MA-HIC-*61*-Ac) in THF at 25 °C.

Table 3 Characteristics of poly(MA-HIC-*61*-Ac) and PMMA standard used in the SAXS measurement and $\langle R_c^2 \rangle_0^{1/2}$ values

Sample	$M_w \times 10^{-5}$[b] (g mol^{-1})	M_w/M_n[b]	d*n*/d*c*[c] (ml g^{-1})	$\langle R_c^2 \rangle_0^{1/2}$ (nm)
Poly(MA-HIC-*61*-Ac)[a]	82.0	1.4_0	0.0842	6.34[d]
Poly(VB-HIC-*62*-H)[e]	8.39	1.4_4	0.0887	5.80[d]
PMMA standard	0.526	1.0_2	0.0851	1.08[f]

Abbreviations: HIC, *n*-hexyl isocyanate; PMMA, poly(methyl methacrylate); SAXS,small-angle X-ray scattering; SEC-MALS, size exclusion chromatography-multiangle laser light scattering; THF, tetrahydrofuran.
[a]Polymerization condition, [MA-HIC-*61*-Ac] = 50.6 mmol l^{-1} and [V-601] = 8.0 mmol l^{-1} at 60 °C for 24 h, conversion = 61%.
[b]Determined by SEC-MALS in THF at 25 °C.
[c]In THF at 25 °C.
[d]Determined by SAXS in THF at 25 °C.
[e]Kikuchi *et al*.[30]
[f]In acetone at 25 °C.

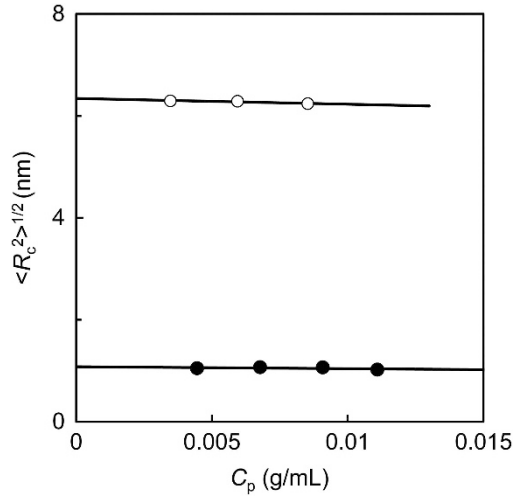

Figure 4 Cross-sectional radius of gyration $\langle R_c^2 \rangle^{1/2}$ as a function of C_p for poly(MA-HIC-*61*-Ac; ○) and PMMA (●) in THF at 25 °C.

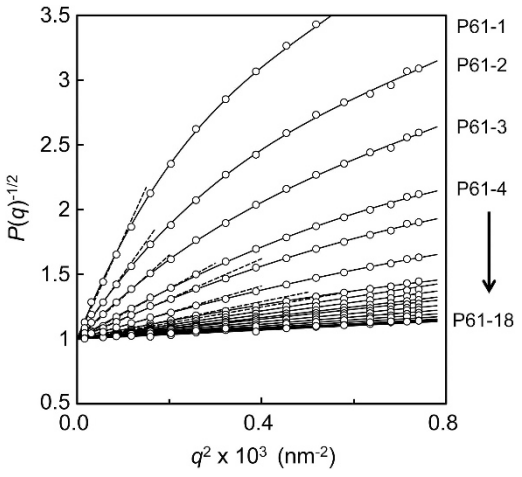

Figure 5 Angular dependence of $P(q)^{-1/2}$ for the indicated fractions of poly(MA-HIC-*61*-Ac) in THF at 25 °C. The broken lines indicate the initial slope.

following equation:

$$\langle R_g^2 \rangle_z^{1/2} = 1.01 \times 10^{-2} M_w^{0.60} \quad \text{(nm)} \tag{4}$$

The power law exponent of 0.60 and the fact that $P(q)$ is described by the Debye function clearly support that the PMMA chain in THF at 25 °C substantially assumes a typical coil-like conformation, which is perturbed by the excluded volume effects in a good solvent.

Cross-section radius of gyration of poly(MA-HIC-*61*-Ac)

Figure 3 shows the cross-sectional Guinier plots of $\ln(q\Delta I(q))$ obtained from the SAXS measurement versus q^2 for poly(MA-HIC-*61*-Ac; $M_w = 82.0 \times 10^5$ g mol^{-1}, $M_w/M_n = 1.40$) in THF at 25 °C at various C_ps. The cross-sectional radius of gyration ($\langle R_c^2 \rangle^{1/2}$) of a straight cylinder may be determined from the slope via the following equation:[36]

$$\ln(q\Delta I(q)) = \ln\frac{k^2 N\pi}{L} - \frac{1}{2}\langle R_c^2 \rangle q^2 \tag{5}$$

Here, $\Delta I(q)$ is the experimental excess scattering intensity, L is the contour length of the cylinder, k is the electron density contrast factor, N is the number of cylinders and q is the scattering vector, which is defined from the scattering angle, θ, and the wavelength, λ, via the following equation:

$$q = \frac{4\pi \sin\theta}{\lambda} \tag{6}$$

Figure 4 presents the C_p dependence of $\langle R_c^2 \rangle^{1/2}$ of poly (MA-HIC-*61*-Ac; ○) in THF at 25 °C. The experimental data for linear PMMA (●) with a $M_w = 5.26 \times 10^4$ g mol^{-1} and a $M_w/M_n = 1.02$ in acetone at 25 °C are also shown in this figure. Extrapolating to $C_p = 0$ gives the $\langle R_c^2 \rangle_0^{1/2}$ of a rod brush and PMMA at an infinite dilution, and the values are listed in Table 3. The value of $\langle R_c^2 \rangle_0^{1/2}$ determined for poly(MA-HIC-*61*-Ac) is slightly larger than that of poly(VB-HIC-*62*-H), which is most likely explained by the experimental fact that the $\langle R_c^2 \rangle_0^{1/2}$ of PMMA is much higher than that of polystyrene ($\langle R_c^2 \rangle_0^{1/2} = 0.311$ nm).[30]

Main chain stiffness of poly(MA-HIC-*61*-Ac)

The value of d*n*/d*c* for poly(MA-HIC-*61*-Ac) in THF at 25 °C is listed in Table 3 and is slightly smaller than poly(VB-HIC-*62*-H). This difference arises from the chemical structure of the main chain. Figure 5 shows the square root plots of $P(q)^{-1/2}$ versus q^2 for poly(MA-HIC-*61*-Ac) determined using SEC-MALS in THF at 25 °C.

Table 4. Characterization results of poly(MA-HIC-*61*-Ac)

Slice number of poly(MA-HIC-61-Ac)	$M_w \times 10^{-6}$ [a] (g mol^{-1})	$N_M \times 10^{-3}$ [b]	$\langle R_g^2 \rangle_z^{1/2}$ [a] (nm)
1	49.2	7.75	216
2	33.5	5.28	174
3	23.2	3.66	140
4	16.0	3.52	108
5	13.5	2.12	96.4
6	10.1	1.59	78.4
7	7.75	1.22	65.9
8	7.00	1.10	61.0
9	6.41	1.01	57.2
10	5.83	0.918	53.3
11	5.35	0.841	49.9
12	4.92	0.774	48.0
13	4.52	0.711	44.6
14	4.08	0.643	41.4
15	3.72	0.586	38.6
16	3.39	0.534	36.4
17	3.09	0.487	34.4
18	2.87	0.451	33.6

Abbreviations: HIC, hexyl isocyanate; SEC-MALS, size exclusion chromatography-multiangle laser light scattering; THF, tetrahydrofuran.
[a]Determined by SEC-MALS in THF at 25 °C.
[b]Weight-averaged degree of polymerization of the main chain, $N_M = M_w/M_{Macromonomer}$, where $M_{Macromonomer}$ is the M_n of the macromonomer.

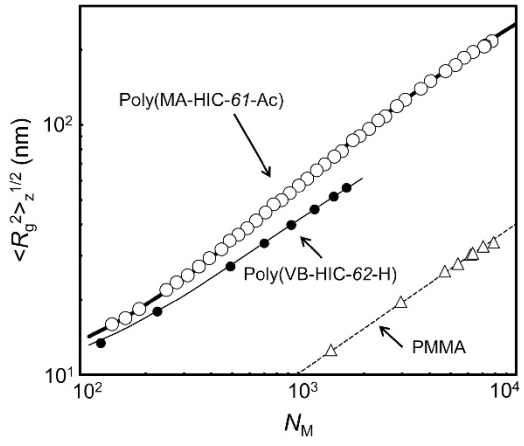

Figure 6 N_M dependence of the measured $\langle R_g^2 \rangle_z^{1/2}$ for poly(MA-HIC-*61*-Ac (○), poly(VB-HIC-*62*-H (●),[30] and PMMA (△) in THF at 25 °C. The solid lines are the theoretical values for the wormlike cylinder model using the parameters indicated in Table 5. The broken lines are calculated from Equation (4).

From the initial slope (represented by broken lines) in these plots, $\langle R_g^2 \rangle_z^{1/2}$ is determined. The determined molecular characteristics of poly(MA-HIC-*61*-Ac) are listed in Table 4.

Figure 6 presents the double logarithmic plot of $\langle R_g^2 \rangle_z^{1/2}$ versus the weight-averaged degree of polymerization of the main chain, $N_M = M_w/M_{Macromonomer}$, where $M_{Macromonomer}$ is the M_n of the macromonomer. The values for linear PMMA (△) and for poly(VB-HIC-*62*-H;●)[30] are also plotted in this figure. The main chain contour length is normalized in this plot. There are two interesting observations to be noted. The first is that the $\langle R_g^2 \rangle_z^{1/2}$ values for poly(MA-HIC-*61*-Ac) are much higher than those for linear PMMA with the corresponding N_M, clearly supporting the idea that the polymethacrylate main chain stiffens because of the densely located side rods. The second is that the main chain of poly(MA-HIC-*61*-Ac) is stiffer than that of poly(VB-HIC-*62*-H), despite having the same side length. This experimental observation demonstrates that the main chain stiffness of the rod brushes is considerably influenced by the primary structure of the main chain.

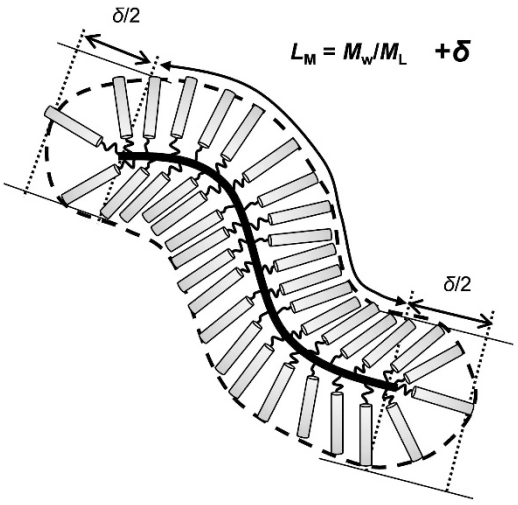

Figure 7 Schematic cartoon of the end effects of side chain (δ) near the ends on the main chain contour length of the rod brush.

To determine the main chain stiffness parameter (λ_M^{-1}) for the poly(MA-HIC-*61*-Ac) chain, the N_M dependence of $\langle R_g^2 \rangle_z^{1/2}$ was analyzed using the cylindrical wormlike chain model with an end effect.[29,30] This model is schematically illustrated in Figure 7, where $\delta/2$ represents the contribution of the side chains near the ends to the main chain contour. Therefore, the main chain contour length, L_M, may be determined from the following equation

$$L_M = \frac{M_w}{M_L} + \delta \tag{7}$$

where M_L is the molecular weight per unit contour length. The mean-square radius of gyration ($\langle R_g^2 \rangle$) of a cylindrical wormlike chain may be expressed by[37]

$$\langle R_g^2 \rangle = \langle R_g^2 \rangle_M + \langle R_c^2 \rangle \tag{8}$$

where $\langle R_g^2 \rangle_M$ is the main chain mean-square radius of gyration of a brush with a contour length L_M. According to Benoit and Doty[38] for the Kratky-Porod chain, the unperturbed $\langle R_g^2 \rangle_M$ of a monodispersed wormlike chain with the L_M and λ_M^{-1} is expressed by:

$$\langle R_g^2 \rangle_M = \frac{L_M}{6\lambda_M} - \frac{1}{4\lambda_M^2} + \frac{1}{4\lambda_M^3 L_M} - \frac{1}{8\lambda_M^4 L_M^2}(1 - \exp(-2\lambda_M L_M)) \tag{9}$$

Equation (9) may also be approximated by:[30]

$$\left(\frac{M}{\langle R_g^2 \rangle_M}\right)^{1/2} = (6\lambda_M M_L)^{1/2}\left(1 + \frac{3M_L}{2}\left(\frac{1}{2\lambda_M} - \frac{\delta}{3}\right)\frac{1}{M}\right) \tag{10}$$

where the maximum error from the exact value is 2% for $\lambda_M L_M > 4$. Equation (10) indicates that $(M/\langle R_g^2 \rangle_M)^{1/2}$ plotted against M^{-1} with $\delta = 2L_{PHIC}$ should provide an upward curve; however, within a limited region, the plot yields a straight line whose intercept and slope allow the two parameters, λ_M^{-1} and M_L, to be evaluated. The L_{PHIC} is

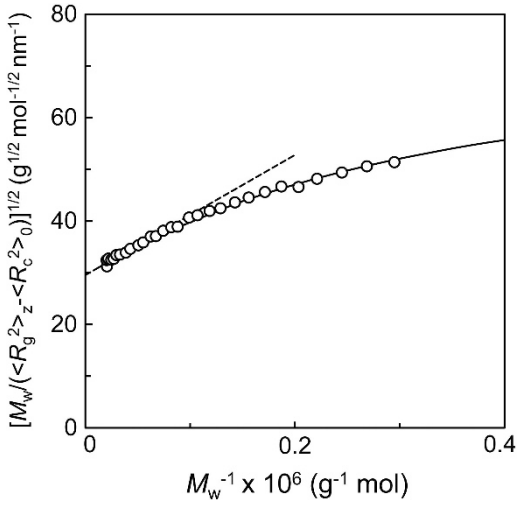

Figure 8 Modified Murakami plots of $(M_w/(\langle R_g^2\rangle_z-\langle R_c^2\rangle_0))^{1/2}$ versus M_w^{-1} constructed form the experimental $\langle R_g^2\rangle_z$ and $\langle R_c^2\rangle_0$ data for poly(MA-HIC-*61*-Ac) in THF at 25 °C. The broken lines show a linear region, and the solid lines are the theoretical value calculated by Equation (10) with the parameters listed in Table 5.

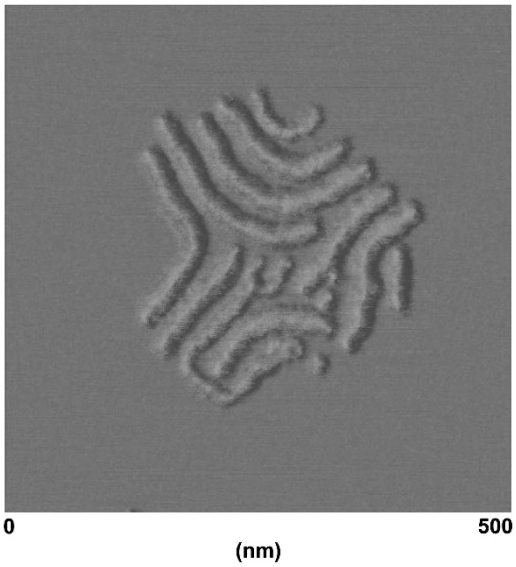

Figure 9 Phase images of AFM measurement for poly(MA-HIC-*61*-Ac); ($M_w = 8.20\times10^6$ g mol^{-1}, $M_w/M_n = 1.40$) on mica at room temperature. A full color version of this figure is available at *Polymer Journal* online.

Table 5. Main chain stiffness parameters of poly(MA-HIC-*61*-Ac) in THF at 25 °C

Sample	λ_M^{-1} (nm)	$M_L\times10^{-4}$ (g mol^{-1} nm^{-1})	δ (nm)[b]
Poly(MA-HIC-*61*-Ac)	197	2.87	21
Poly(VB-HIC-*62*-H)[a]	59	3.15	22

Abbreviations: PHIC, poly(*n*-hexyl isocyanate); THF, tetrahydrofuran.
[a]Kikuchi *et al.*[30]
[b]Calculated from $\delta = 2L_{PHIC}$, where $L_{PHIC} = M_0N_s/M_{L,PHIC}$, with $M_0 = 127.18$ g mol^{-1} and $M_{L,PHIC} = 725$ g mol^{-1} nm^{-1} in THF at 25 °C.[29]

the contour length of a PHIC side chain and may be calculated using $L_{PHIC} = M_0N_s/M_{L,PHIC}$, where M_0 is the molecular weight of HIC and $M_{L,PHIC}$ is the molecular weight per unit contour length of PHIC in THF at 25 °C.[29]

Figure 8 presents the plot of $(M_w/\langle R_g^2\rangle_M)^{1/2}$ against M_w^{-1}, which was constructed from the experimental data ($\langle R_g^2\rangle_M = \langle R_g^2\rangle_z - \langle R_c^2\rangle_0$). These plots provide an upward curve, but when $8 > \lambda_M L_M > 4$, the data follow a straight line (indicated in broken lines), which yields $\lambda_M^{-1} = 197$ nm and $M_L = 2.87\times10^4$ g mol^{-1} nm^{-1}. The solid line shown in Figure 8 is the theoretical line recalculated from Equation (10) using the determined parameters of λ_M^{-1} and M_L. The contour length per backbone monomer (l_M) calculated from $l_M = M_{Macromonomer}/M_L$ for the brush is *ca.* 0.22 nm. The value of l_M is intermediate between the all-*trans* and gauche conformations of the main chain. The model parameters characteristic of the dimensional properties of poly(MA-HIC-*61*-Ac) chain in THF at 25 °C are summarized in Table 5, along with those of poly(VB-HIC-*62*-H).

The comparison of the experimental data of poly(MA-HIC-*61*-Ac) with the theoretical curve (denoted by the thick solid line) calculated from Equations (7)–(9) is shown in Figure 6. The theoretical curve quantitatively describes the dimensional properties of poly (MA-HIC-*61*-Ac). The highest M_w is 49.2×10^6, as listed in Table 4, which corresponds to the Kuhn segment number $n_K = L_M\lambda_M = 8.7$. Therefore, the excluded volume effects for the brush chain are very small and may be substantially ignored in the M_w region investigated in this study.

Figure 9 shows the AFM phase image of poly(MA-HIC-*61*-Ac; $M_w = 8.2\times10^6$ g mol^{-1}, $M_w/M_n = 1.40$) on mica at room temperature. A single, cylindrical, brush-like macromolecule on the mica surface is clearly observed. The trajectory analysis of the image was performed using the '2D Single Molecules' software developed by Roiter and Minko,[39] and determined λ_M^{-1} to be 180 on a two-dimensional state. This value may be interestingly comparable with that ($\lambda_M^{-1} = 197$ nm) in THF at 25 °C.

The most interesting and important experimental finding from this study is that the main chain stiffness of the rod brushes is considerably influenced by the chemical structure of the main chain. The λ_M^{-1} of the polymethacrylate main chain is approximately three times larger than that of the polystyrene main chain, irrespective of both having the same PHIC length. The linear polystyrene and PMMA are originally flexible polymers in solution and have $\sim$2.3[37] and 5.8 nm[40] in values for the stiffness parameter, respectively. In the following, some plausible reasons for the difference in the stiffness between these polymers are discussed.

The chain stiffness of brush polymers has been theoretically investigated by several researchers.[23,41–43] According to Nakamura and Norisuye,[23] the stiffness parameter is a function of the sum of the short range and long range interactions, which is given by the equation:

$$\lambda_M^{-1} = \lambda_0^{-1} + \lambda_s^{-1} \quad (11)$$

Here, λ_0^{-1} is the intrinsic backbone stiffness, including the contributions from the non-excluded volume interactions between the main-chain and side-chain residues near the main chain (short range interaction, that is, steric hindrance effects on the free rotation of the main chain), and λ_s^{-1} is related to the excess free energy resulting from the collisions among the side chains, that is, the excluded volume interaction. There are three plausible interpretations for the experimental result. The first is that the α-methyl group in the main chain of poly(MA-HIC-*61*-Ac) may restrict the rotation of the side rod. In fact, the PMMA main chain is originally stiffer than

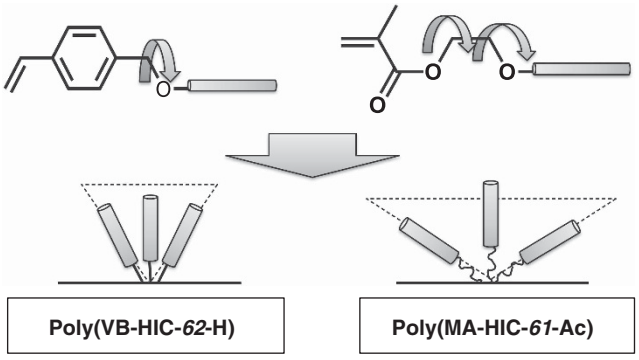

Scheme 3 Schematic cartoons showing the difference in the effective excluded-volume effects produced among the side rods between poly(VB-HIC-*62*-H) and poly(MA-HIC-*61*-Ac).

polystyrene, as mentioned above. Therefore, the PMMA chain may be more susceptible to the effects of the side chain than polystyrene. Based on Equation (11), this effect may result in the increase of λ_0^{-1}. However, such a short range interaction quickly decreases with increasing side chain length. The second is the solvent quality difference of THF between the PMMA and polystyrene main chains. There is an experimental observation that PHIC dissolves in styrene but does not in MMA. This result likely implies that larger repulsive interactions of PMMA with PHIC than those of polystyrene and PHIC may occur. This effect results in the increase of λ_s^{-1}. However, the collision frequency among the main chain and side PHIC chains is much lower than that among the densely located side chains. Therefore, the two effects mentioned above are practically small for the present rod brushes that have long side chains. The third is the difference in the extent of the excluded volume effects produced among the side rods. This effect changes the value of λ_s^{-1}. The excluded volume interactions produced among the side chains may be a function of the strength of the interaction and the collision probability. In this study, the side chains of the brushes have the same chemical natures, that is, the same strength of interaction. Therefore, the higher value of λ_M^{-1} in the PMMA main chain than in the polystyrene likely results from the increase of collision probability. This situation is schematically illustrated in Scheme 3. In the poly(MA-HIC-*61*-Ac) chain, a freely rotating oxyethylene chain is located as a spacer between the methacryloyloxy main chain and the PHIC side chain. This flexible segment may produce somewhat larger effective excluded volume effects among the rods compared with poly(VB-HIC-*62*-H). Currently, this effect most likely explains the present experimental observations. The systematic studies to clarify the influence of the α-methyl group and flexible spacer on the main chain stiffness of the rod brushes are currently in progress and will be reported soon.

CONCLUSION

The dimensional properties of cylindrical rod brushes consisting of a polymethacrylate main chain were studied using static light and SAXS techniques in THF at 25 °C. The N_M dependence of $\langle R_g^2 \rangle_z$ was quantitatively described in terms of the wormlike cylinder model taking into account the end effect. The main chain stiffness parameter, λ_M^{-1}, of poly(MA-HIC-*61*-Ac) was determined to be 197 nm, which was approximately three times greater than that of poly(VB-HIC-*62*-H) that has a polystyrene main chain, despite having the same side rods. The much greater main chain stiffness in poly(MA-HIC-*61*-Ac) chain was believed to result from the larger effective excluded volume effects resulting from the freely rotating spacer between the main chain and side rod. A single rod brush of poly(MA-HIC-*61*-Ac) on a mica surface was clearly observed using AFM to reasonably demonstrate the cylindrical rod brushes.

ACKNOWLEDGEMENTS

This study was supported in part by Grants-in-Aid from the Ministry of Education, Science, Sports and Culture of Japan (16550105) and (19550117), The Foundation for Japanese Chemical Research and the Saneyoshi Scholarship Foundation, which are gratefully acknowledged. The authors thank Mrs Naoya Mashiko and Koichiro Shibata, Yamagata University, for the AFM measurement.

1 Ito, K. Polymeric design by macromonomer technique. *Prog. Polym. Sci.* **23,** 581–620 (1998).
2 Zhang, M. & Müller, A. H. E. Cylindrical polymer brushes. *J. Polym. Sci., Part A: Polym. Chem.* **43,** 3461–3481 (2005).
3 Sheiko, S. S., Sumerlin, B. S. & Matyjaszewski, K. Cylindrical molecular brushes: synthesis, characterization, and properties. *Prog. Polym. Sci.* **33,** 759–785 (2008).
4 Ito, K. & Kawaguchi, S. Poly(macromonomers): homo- and copolymerization branched polymers. *Adv. Polym. Sci.* **142,** 129–178 (1999).
5 Kawaguchi, S. & Ito, K. Dispersion polymerization. *Adv. Polym. Sci.* **175,** 299–328 (2005).
6 Runge, M. B. & Bowden, N. B. Synthese. *J. Am. Chem. Soc.* **129,** 10551–10560 (2007).
7 Xia, Y., Olsen, B. D., Kornfield, J. A. & Grubbs, R. H. Efficient synthesis of narrowly dispersed brush copolymers and study of their assemblies: the importance of side chain arrangement. *J. Am. Chem. Soc.* **131,** 18525–18532 (2009).
8 Rzayev, J. Synthesis of polystyrene−polylactide bottlebrush block copolymers and their melt self-assembly into large domain nanostructures. *Macromolecules* **42,** 2135–2141 (2009).
9 Huang, K. & Rzayev, J. Well-defined organic nanotubes from multicomponent bottlebrush copolymers. *J. Am. Chem. Soc.* **131,** 6880–6885 (2009).
10 Djalali, R., Li, S.-Y. & Schmidt, M. Amphipolar core−shell cylindrical brushes as templates for the formation of gold clusters and nanowires. *Macromolecules* **35,** 4282–4288 (2002).
11 Du, J.-Z., Tang, L.-Y., Song, W.-J., Shi, Y. & Wang, J. Evaluation of polymeric micelles from brush polymer with poly(ε-caprolactone)-b-poly(ethylene glycol) side chains as drug carrier. *Biomacromolecules* **10,** 2169–2174 (2009).
12 Zhang, W., Li, Y., Liu, L., Sun, Q., Shuai, X., Zhu, W. & Chen, Y. Amphiphilic toothbrushlike copolymers based on poly(ethylene glycol) and poly(ε-caprolactone) as drug carriers with enhanced properties. *Biomacromolecules* **11,** 1331–1338 (2010).
13 Lee, H.-i., Jakubowski, W., Matyjaszewski, K., Yu, S. & Sheiko, S. S. Cylindrical core−shell brushes prepared by a combination of ROP and ATRP. *Macromolecules* **39,** 4983–4989 (2006).
14 Gao, H. & Matyjaszewski, K. Synthesis of molecular brushes by "grafting onto" method: combination of ATRP and click reactions. *J. Am. Chem. Soc.* **129,** 6633–6639 (2007).
15 Jha, S., Dutta, S. & Bowden, N. B. Synthesis of ultralarge molecular weight bottlebrush polymers using Grubbs' catalysts. *Macromolecules* **37,** 4365–4374 (2004).
16 Iha, R. K., Wooley, K. L., Nystrom, A. M., Burke, D. J., Kade, M. J. & Hawker, C. J. Applications of orthogonal "click" chemistries in the synthesis of functional soft materials. *Chem. Rev.* **109,** 5620–5686 (2009).
17 Wintermantel, M., Schmidt, M., Tsukahara, Y., Kajiwara, K. & Kohjiya, S. Rodlike combs. *Macromol. Rapid Commun.* **15,** 279–284 (1994).
18 Wintermantel, M., Gerle, M., Fischer, K., Schmidt, M., Wataoka, I., Urakawa, H., Kajiwara, K. & Tsukahara, Y. Molecular bottlebrushes. *Macromolecules* **29,** 978–983 (1996).
19 Zhang, B., Gröhn, F., Pedersen, J. S., Fischer, K. & Schmidt, M. Conformation of cylindrical brushes in solution: effect of side chain length. *Macromolecules* **39,** 8440–8450 (2006).
20 Terao, K., Takeo, Y., Tazaki, M., Nakamura, Y. & Norisuye, T. Polymacromonomer consisting of polystyrene. Light scattering characterization in cyclohexane. *Polym. J.* **31,** 193–198 (1999).
21 Terao, K., Hokajo, T., Nakamura, Y. & Norisuye, T. Solution properties of polymacromonomers consisting of polystyrene. 3. Viscosity behavior in cyclohexane and toluene. *Macromolecules* **32,** 3690–3694 (1999).
22 Hokajo, T., Terao, K., Nakamura, Y. & Norisuye, T. Solution properties of polymacromonomers consisting of polystyrene - V. Effect of side chain length on chain stiffness. *Polym. J.* **33,** 481–485 (2001).
23 Nakamura, Y. & Norisuye, T. Backbone stiffness of comb-branched polymers. *Polym. J.* **33,** 874–878 (2001).
24 Nakamura, Y. & Norisuye, T. in *Soft Matter Characterization* (eds Borsali, R. & Pecora, R.) Ch. 5 (Springer Science+Business Media, LLC, New York, 2008).

25 Radke, W., Roos, S., Stein, H. M. & Müller, A. H. E. Acrylic thermoplastic elastomers and comb-shaped poly(methyl methacrylate) via the macromonomer technique. *Macromol. Symp.* **101,** 19–27 (1996).
26 Ito, K., Tomi, Y. & Kawaguchi, S. Poly(ethylene oxide) macromonomers. 10. Characterization and solution properties of the regular comb polymers with polystyrene main chains and poly(ethylene oxide) side chains. *Macromolecules* **25,** 1534–1538 (1992).
27 Kawaguchi, S., Akaike, K., Zhang, Z. M., Matsumoto, H. & Ito, K. Water soluble bottlebrushes. *Polym. J.* **30,** 1004–1007 (1998).
28 Kawaguchi, S., Maniruzzaman, M., Katsuragi, K., Matsumoto, H., Iriany, Ito, K., Hugenberg, N. & Schmidt, M. Fluorescence probe and scanning force microscopic studies of water soluble comb-shaped copolymers consisting of a hydrophobic poly (p-alkylstyrene) main chain and hydrophilic poly(ethylene oxide) grafted chains. *Polym. J.* **34,** 253–260 (2002).
29 Kikuchi, M., Mihara, T., Jinbo, Y., Izumi, Y., Nagai, K. & Kawaguchi, S. Characterization of rodlike poly(n-hexyl isocyanate) macromonomers and their polymacromonomers by light scattering, SAXS, intrinsic viscosity, and scanning force microscopy. *Polym. J.* **39,** 330–341 (2007).
30 Kikuchi, M., Lien, L. T. N., Narumi, A., Jinbo, Y., Izumi, Y., Nagai, K. & Kawaguchi, S. Conformational properties of cylindrical rod brushes consisting of a polystyrene main chain and poly(n-hexyl isocyanate) side chains. *Macromolecules* **41,** 6564–6572 (2008).
31 Kawaguchi, S., Mihara, T., Kikuchi, M., Lien, L. T. N. & Nagai, K. Synthesis of methacrylate-ended poly(n-hexyl isocyanate) rodlike macromonomers and their radical copolymerization behavior. *Macromolecules* **40,** 950–958 (2007).
32 Lien, L. T. N., Kikuchi, M., Narumi, A., Nagai, K. & Kawaguchi, S. Preparation of α-, ω-end-functionalized poly(n-hexyl isocyanate) heterotelechelics. *Polym. J.* **40,** 1105–1112 (2008).
33 Lien, L. T. N., Kikuchi, M., Narumi, A., Nagai, K. & Kawaguchi, S. Synthesis of oligo(oxyethylene) methacrylate-ended poly(n-hexyl isocyanate) rodlike macromonomers and their radical copolymerization behavior with methyl methacrylate. *Polym. J.* **40,** 1113–1120 (2008).
34 Takaeda, Y., Yoshizaki, T. & Yamakawa, H. Mean-square optical anisotropy of oligo- and poly(methyl methacrylate)s in dilute solutions. *Macromolecules* **26,** 3742–3749 (1993).
35 Kawaguchi, S., Soewito, D. P. & Ito, K. Characterization of randomly branched polystyrenes by multi-angle laser light scattering-size exclusion chromatography. *Kobunshi Ronbunshu* **54,** 923–929 (1997).
36 Glatter, O. & Kratky, O. *Small Angle X-ray Scattering* (Academic Press, London, 1982).
37 Konishi, T., Yoshizaki, T., Saito, T., Einaga, Y. & Yamakawa, H. Mean-square radius of gyration of oligo- and polystyrenes in dilute solutions. *Macromolecules* **23,** 290–297 (1990).
38 Benoit, H. & Doty, P. Light scattering from non-gaussian chains. *J. Phys. Chem.* **57,** 958–963 (1953).
39 Roiter, Y. & Minko, S. 2D single molecules. Available for download at http://people.clarkson.edu/~sminko/.
40 Tamai, Y., Konishi, T., Einaga, Y., Fujii, M. & Yamakawa, H. Mean-square radius of gyration of oligo- and poly(methyl methacrylate)s in dilute solutions. *Macromolecules* **23,** 4067–4075 (1990).
41 Birshtein, T. M., Borisov, O. V., Zhulina, Y. B., Khokhlov, A. R. & Yurasova, T. A. Conformations of comb-like macromolecules. *Vysokomol. Soedin.* **A29,** 1169–1174 (1987).
42 Fredrickson, G. H. Surfactant-induced lyotropic behavior of flexible polymer solutions. *Macromolecules* **26,** 2825–2831 (1993).
43 Zhulina, E. B. & Vilgis, T. A. Scaling theory of planar brushes formed by branched polymers. *Macromolecules* **28,** 1008–1015 (1995).